A Finite Element Method Study of Delamination at the Interface of the TSV Interconnects

S. Papaleo and H. Ceric
Christian Doppler Laboratory for Reliability Issues in Microelectronics at the
Institute for Microelectronics TU Wien
Gußhausstraße 27-29, 1040 Wien, Austria
phone: +43 (1) 58801 - 36037, Email: {papaleo|ceric}@iue.tuwien.ac.at

***Abstract*—Through Silicon Vias (TSVs) are the interconnections in three dimensional integrated circuits responsible for the vertical lines inside the dies. In particular, the open TSV has been developed in order to reduce thermo-mechanical issues. This interconnect structure has interfaces where the possibility of a device failure due to delamination needs to be considered. The Critical Energy Release Rate G_c determines the condition for a fracture to propagate. When the Energy Release Rate G exceeds G_c, a fracture will propagate. Experimental measurements were used to calculate G_c. The experimental G_c, was calculated at the interface between silicon dioxide and tungsten; materials used for Open TSVs. We have developed a model to calculate the G and compared the experimental data with our results. The results obtained are in good agreement with experimental measurements. Therefore, the model developed provides a convenient tool for the study of delamination issues in TSVs.**

***Index Terms*—4PB, delamination, FEM, interface fracture energy, TSV**

I. Introduction

The 3D integration technology is one of the most promising approaches for semiconductor device development. 3D interconnects permit higher performance by increasing the integration density of the technology [1]. The TSVs are vertical 3D connections of the stacked semiconductor dies.

Due to the mismatched thermal expansion coefficients, the addition of large metal vias in the middle of a die generates high mechanical stress. The Open TSV technology was introduced to avoid the failure due to thermo-mechanical issues induced by the material properties [1]. Unlike a filled TSV, in an Open TSV, the metal layer can expand in the hollow via reducing the probability of failure.

During the fabrication process of the TSV different material layers are deposited. The sidewall area of the TSV consists of isolation, metallization, and passivation layers [1]. In an Open TSV a typical conductor material is tungsten. Due to deposition and thermal processes, it has a high value of tensile intrinsic stress [2]. The stress in the layers can be sufficiently high to degrade the performance and to induce crack or delamination in the TSVs. Particularly at the interfaces of the TSV the possibility of a mechanical failure needs to be considered. The energy release rate G is used for the prediction of the failure of the interfaces. If the G exceeds the value G_c the interface delamination will progress [3]. The four point bend (4PB) setup was used to determine the experimental values of G_c. G_c was measured at different interfaces of Open TSVs. In the present work we use COMSOL Multiphysics [4] Finite Element Method (FEM) to simulate the 4PB technique and to calculate the G. The G values obtained were compared with the experimental data.

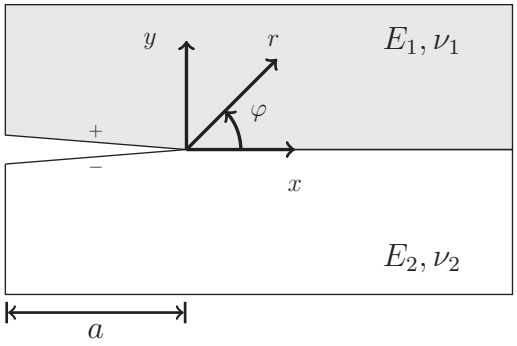

Fig. 1: Tip of a bimaterial crack.

II. Theory

We have considered bimaterial cracks as fractures at the interface between two materials with different elastic constants. Material compounds, adhesive joints or interfaces of composite materials can be subject to this kind of failure. By definition, the G value is the released energy during a crack advance. By considering the two-dimensional geometry in Fig. 1, during the delamination, at the right side of the crack tip along the interface, the shear and normal stresses act. If the delamination

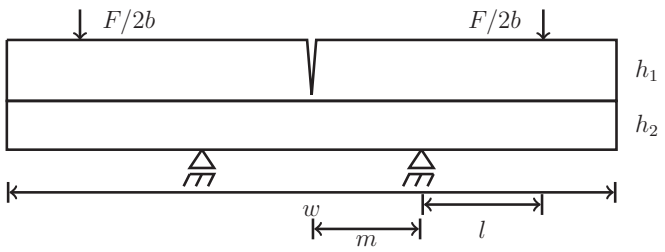

Fig. 2: Schematic representation of the studied system. On the top a force (F) was applied, and at the bottom two fixed points were used as bearings.

978-1-4673-9137-5/16/$31.00 ©2016 IEEE

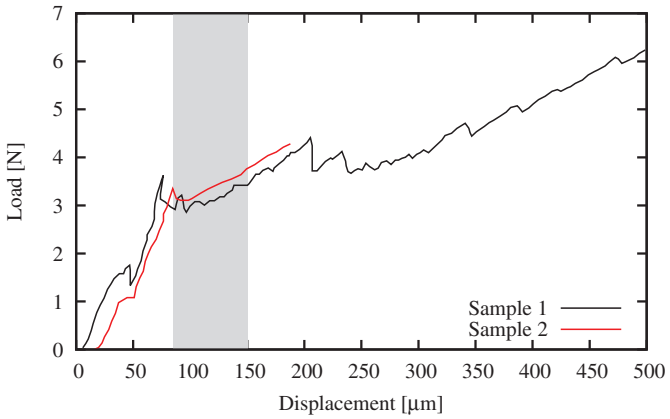

Fig. 3: Experimental results of the samples 1 and 2. The gray area indicates the steady state region where the delamination appears.

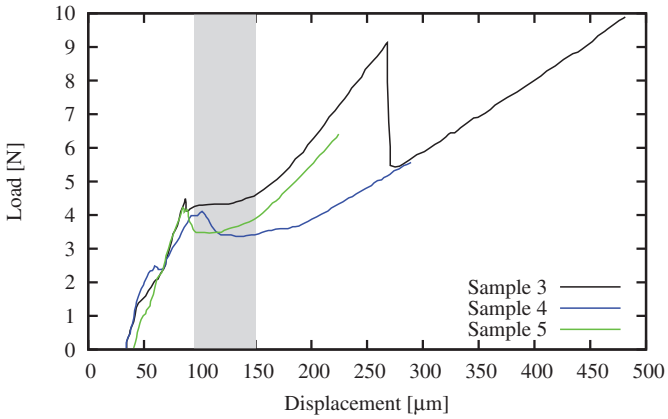

Fig. 4: Experimental results of the samples 3, 4, and 5. The gray area indicates the steady state area where the delamination appears.

is going to happen only along the interface, the stresses are given as

$$(\sigma_y + \tau_{xy})_{\varphi=0} = \frac{K(r/2a)^{i\varepsilon}}{\sqrt{2\pi r}}, \tag{1}$$

where σ_y is the normal stress, τ_{xy} is the shear stress, a the crack length, and φ the angle and r the radius in polar coordinates for the stress distribution as indicated in Fig. 1 [3]. The symbol ε denotes the bimaterial constant and is defined as

$$\varepsilon = \frac{1}{2} ln \frac{\mu_2\kappa_1 + \mu_1}{\mu_1\kappa_2 + \mu_2}, \tag{2}$$

with $\mu_n = E_n/2(1+\nu_n)$ and $\kappa_n = 3 - 4\nu_n$. E is the Young Modulus, ν is the Poisson ratio, and n indicates the material. The displacements along the interface is described as

$$(v^+ - v^-) + i(u^+ - u^-) = \frac{c_1 + c_2}{2\cosh(\pi\varepsilon)} \frac{K(r/2a)^{i\varepsilon}}{1 + 2i\varepsilon} \sqrt{\frac{r}{2\pi}}, \tag{3}$$

where u and v are the displacements in x and y directions, and c_n is defined as $c_n = (1+\kappa_n)/\mu_n$ [3]. The positive sign on the displacement indicates the upper crack face and the negative the lower crack face (c.f. Fig. 1).
The stress complex intensity factor is defined as

$$K = K_1 + iK_2. \tag{4}$$

Unlike a crack in a homogeneous material the stress intensity factors does not indicate neither the opening mode (mode I) nor the sliding mode (mode II) [3], but mixed mode. The stress intensity factor K_1 is not only associated with the normal stress in the interface but also with the shear stress. The same is the case for K_2. The stress along the interface can be written explicitly, by separating real and imaginary parts. Therefore the mix mode dependence is shown:

$$\begin{aligned} \sigma_y &= \tfrac{1}{\sqrt{2\pi r}}\{K_1 \cos[\varepsilon ln(r/2a)] - K_2 \sin[\varepsilon ln(r/2a)]\} \\ \tau_{xy} &= \tfrac{1}{\sqrt{2\pi r}}\{K_1 \sin[\varepsilon ln(r/2a)] + K_2 \cos[\varepsilon ln(r/2a)]\} \end{aligned} \tag{5}$$

Thus, for a delamination, both modes are connected with each other.

In the case of homogeneous materials where $c_1 = c_2$ the two modes are separable [3].

For a two-dimensional system, the energy release rate G during crack growth in the interface is defined [3] as

$$G = -\frac{d\Pi}{da}. \tag{6}$$

Π is the elastic potential and can be calculated by using Eq. 1 and Eq. 3 [3]. Solving the Equation 6 we get

$$G = \frac{(c_1 + c_2)(K_1^2 + K_2^2)}{16\cosh^2(\pi\varepsilon)}. \tag{7}$$

As can be seen the G can be calculated only determining the stress intensity factors. The critical energy release rate G_c for different interfaces can be found in literature [5]. For an accurate failure prediction the G_c needs to be experimentally measured for the desired system. The condition for a fracture to propagate is defined by

$$G \geq G_c. \tag{8}$$

The knowledge of G_c is necessary to study the conditions for the delamination propagation at the interface.

III. 4PB Specimen

There are several methods for measuring G_c which employ different sample geometries. The thin film delamination can be generated using some driving force or stored energy in the films [5]. The Fraunhofer Institute for Electronic Nano Systems (ENAS) used a 4PB specimen [6] to determine the experimental G_c.

In microelectronics, the fracture at interfaces between different materials is a critical phenomenon for device reliability. Different techniques are available for reliability analysis. The 4PB technique is the most popular adhesion test employed to characterize interface cracks. For such fractures, normal and shear stress act along the crack and the mixed mode condition prevails.

The four point beam setup used is illustrated in Fig. 2. The 4PB technique consists in a bimaterial flexural beam with a

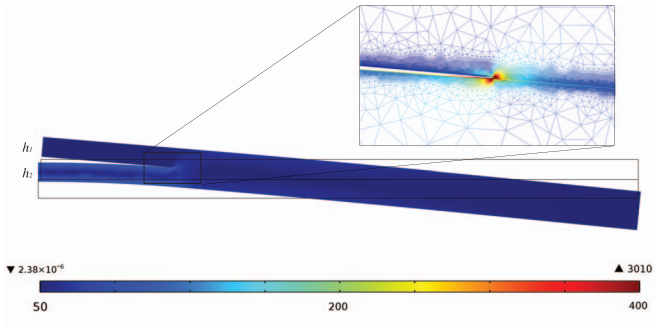

Fig. 5: FEM simulation of 4PB test. The legend indicates the Von Mises Stress (MPa). Due to the boundary condition the development of the stress in the bottom layer is observable. In the inset the mesh used is shown.

notch on the top layer. For the bimaterial beam two silicon wafers were used to sandwich the film of interest. Under the silicon top layer indicated with h_1(Fig. 2) a silicon dioxide layer with a thickness of 500nm was placed. Subsequently, at the silicon dioxide layer a tungsten layer with a thickness of 200nm and a titanium nitride layer with a thickness of 11nm were placed. On the top of the silicon layer indicated with h_2 an adhesive was laid for linking the top layer h_1. At the interfaces of three samples, between the silicon dioxide and titanium nitride, an additional titanium layer with a thickness of 25nm was deposited. The deposition process of the titanium nitride layer, the thickness of the layers, and the samples including the titanium layer are presented in Table I. All the samples have a length w of 44mm and a depth b of 3.5mm.

In the 4PB method a constant load F and two fixed points are applied at the sample as shown in the Fig. 2. By recording the load as a function of displacement a plateau was obtained when the crack interface reached the steady state. In this regime G is independent of the crack length and indicates G_c [6].

In the 4PB technique, the Euler-Bernoulli beam theory in plane strain condition is applied [6], and the critical energy release rate G_c can be calculated as

$$G_c = \frac{3F_c^2 l^2}{2E_{Si}b^2}\left[\frac{1}{h_2^3} - \frac{1}{h_1^3 + h_2^3 + 3h_1h_2(h_1+h_2)}\right] \quad (9)$$

where F_c is the force measured at the steady state of the plots in Fig. 3 and Fig. 4. E_{Si} is the Young modulus of silicon and the other parameters are indicated in Fig. 2.

Sample	h_1 [μm]	h_2 [μm]	% Del.	Comments
1	726.3	684.6	28	CVD-TiN with Ti
2	725.7	684.4	7	CVD-TiN without Ti
3	725.5	688.3	78	CVD-TiN with Ti
4	726	698.7	89	CVD-TiN without Ti
5	724.7	683.3	84	PVD-TiN with Ti

TABLE I: Geometry of the samples. The thickness h_2 includes the thickness of the adhesive. The comments indicate the kind of deposition process and the presence or absence of the titanium layer.

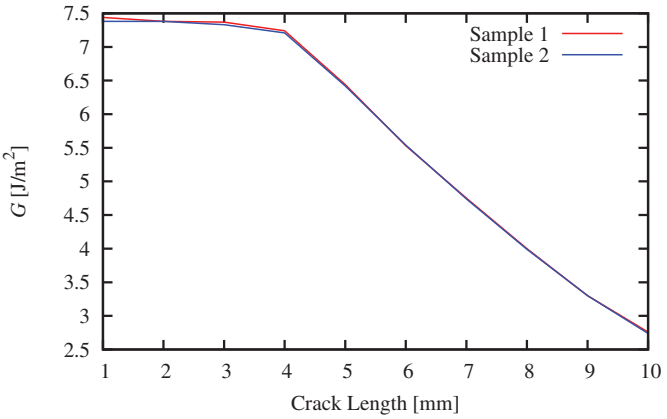

Fig. 6: G obtained from FEM simulations. We simulated crack length in the range from 1nm to 10nm.

IV. Simulation

The 4PB technique was simulated using the FEM COMSOL. The geometry used for the experiment has been reproduced in two-dimensional simulations. Due to the symmetry conditions in the 4PB test, it is sufficient to consider only half of the structure as shown in Fig. 5. All the materials are assumed to be linear elastic. On the left side of the Fig. 5 a symmetry condition was applied and a fixed point and a load point were applied as in experiment. Near the crack tip, a very fine mesh was used. The simulations have been started with an interface crack length of 1mm, which has been increased by steps of 1mm until reaching the desired value.

In Fig. 5 the results of a simulation with a=5mm is shown. Due to the boundary condition the Von Mises Stress is mainly generated at the h_2 layer. The stress distribution at the interface crack opening is described by Eq. 1. For every crack length we collected the values for σ_y and τ_{xy} as a function of r.

V. Energy Release Rate Determination

The energy release rate can be calculated determining the values of K_1 and K_2 (see Eq.7). The stress intensity factors are obtainable using the stress at the head for the right crack tip (Fig. 1) which is described by Eq. 5. The equation for σ_y is multiplied by $\cos[\varepsilon ln(r/2a)]$ and added to the equation for τ_{xy} previously multiplied by $\sin[\varepsilon ln(r/2a)]$ [7]. The resulting equation is denoted as σ_1 and represent the combined stress

$$\sigma_1 = \sigma_y \cos[\varepsilon ln(r/2a)] + \tau_{xy}\sin[\varepsilon ln(r/2a)] = \frac{K_1}{\sqrt{2\pi r}}. \quad (10)$$

Analogously τ_{xy} is multiplied by $\cos[\varepsilon ln(r/2a)]$ and added to σ_y multiplied by $\sin[\varepsilon ln(r/2a)]$. σ_2 denotes the combined stress as

$$\sigma_2 = -\sigma_y \cos[\varepsilon ln(r/2a)] + \tau_{xy}\sin[\varepsilon ln(r/2a)] = \frac{K_2}{\sqrt{2\pi r}}. \quad (11)$$

Now, σ_1 and σ_2 can be calculated by using the σ_y and τ_{xy} obtained from the FEM simulations. The stress intensity factors K_1 and K_2 were calculated from a linear regression fit of σ_1 versus r and σ_2 versus r, respectively [7] [8]. The

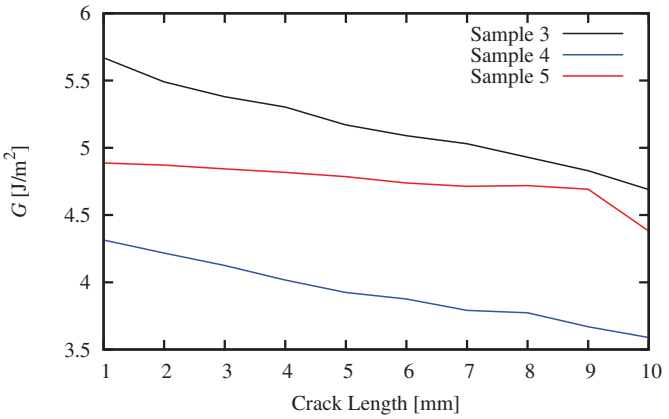

Fig. 7: G obtained from FEM simulations. We simulated crack length in the range from 1nm to 10nm.

values K_1 and K_2 were used to calculate G by using Eq. 7. We applied this procedure for every simulated crack length in the range from 1nm to 10nm.

VI. Results

Fig. 6 displays the G calculated at every crack length a for the samples 1 and 2 (Table I). As the crack approaches the fixed point of the 4PB test (4mm from the center of these samples, m in the Fig. 2), the G decreases [9].
The G for every crack length a for the samples 3,4 and 5 (Table I) is shown in Fig. 7. Here the decrease of G is less pronounced than in for samples 1 and 2. The value m=10mm as in the experiment was used and the simulation were made until the reaching of crack length of a=10mm. The different line slopes are due to the different thicknesses and interfaces of the sample employed.

The experimental G_c was determined by using the average of the loads in a steady state range. Also for the FEM results an average of G_c was determined. In particular, for the samples 1 and 2, G_c was calculated in a range of crack lengths from 1mm to 4mm and for the samples 3,4 and 5 in a range of crack lengths from 3mm to 9mm.

In Table II the G_c obtained from experimental and simulation data are compared. For the samples 1 and 2 the FEM results differ from the experiments results. We have attributed this inaccuracy to the behaviour observable in Fig. 3. In these load-displacement plots no clean steady state regions are observable. The discontinuous ties of the load plots are due to unstable crack propagation. We suppose that due to some defects or imperfect adhesion of the layers the delamination does not emerge evenly. This is also perceptible considering the percent of delamination in these two samples in comparison to the other samples with the same composition (Table I). Instead, the FEM results for the samples 3,4 and 5 appear closer, as observable in Table II. The G_c for the samples 3 and 4 are very close to the experimental values. Also here, we assume that is due to a better adhesion in a longer region and thus a more pronounced steady state load area. In Fig. 4 a recognizable constant load created from the delamination is

Sample	Experimental $G_c[J/m^2]$	Simulation $G_c[J/m^2]$
1	5.95	7.36
2	5.9	7.33
3	4.6	5.10
4	3.5	3.88
5	3.9	4.75

TABLE II: G_c calculated from experimental data and simulations. The G_c calculated for the samples 3, 4, and 5 are in good agreement with the G_c of the experiment.

observable. The FEM result for the sample 5 is less accurate but still in a good range.

From the experimental data and simulation results no influence due to the inclusion of the titanium layer (Table I) are negligible.

VII. Conclusion

We described the FEM method used to calculate the energy release rate G at the interface between two materials. The 4PB technique can be simulated by considering a simplified structure. From the FEM simulations, the stress at the interface was obtained and used to calculate the energy release rate G. The FEM results are strongly dependent on the quality of the experimental data. The calculation of G_c necessitates a load-displacement plot where a steady state load is clearly definable and observable. This study demonstrated the efficiency of the FEM simulation and how it can be used to calculate G for different boundary conditions and geometries of the TSV structure, where the delamination is an issue.

Acknowledgment

The authors want to thank the Fraunhofer Institute (ENAS) for the measurement data.

This work was supported by the Christian Doppler Laboratory for Reliability Issues in Microelectronics, project number 5117.

References

[1] J. Kraft, F. Schrank, J. Teva, J. Siegert, G. Koppitsch, C. Cassidy *et al.*, "3D Sensor Application with Open Through Silicon Via Technology," *Proc. ECTC*, pp. 560–566, May 2011.

[2] C. Krauss, S. Labat, S. Escoubas, O. Thomas, S. Carniello, J. Teva, and F. Schrank, "Stress Measurements in Tungsten Coated Through Silicon Vias for 3D Integration," *Thin Solid Films*, vol. 530, pp. 91 – 95, 2013.

[3] D. Gross and T. Seelig, *Fracture Mechanics*, ser. Mechanical Engineering Series. Springer-Verlag Berlin Heidelberg, 2011.

[4] COMSOL. Comsol Multiphysics Version 5.1. [Online]. Available: https://www.comsol.eu

[5] A. A. Volinsky, N. R. Moody, and W. W. Gerberich, "Interfacial Toughness Measurements for Thin Films on Substrates," *Acta Mater.*, vol. 50, pp. 441–466, 2002.

[6] P. Charalambides, J. Lund, A. Evans, and R. McMeeking, "A Test Specimen for Determing the Fracture Resistance of Bimaterial Interfaces," *Journal of Applied Mechanics*, vol. 56, no. 1, pp. 77–82, 1989.

[7] R. A. Naik and J. Crews, John H., "Determination of Stress Intensity Factors for Interface Cracks Under Mixed-Mode Loading," *Paper presented at the ASTM National Symposium on Fracture Mechanics*, 1992.

[8] M. Kuna, *Finite Elements in Fracture Mechanics*, ser. Solid Mechanics and Its Applications. Springer Netherlands, 2013.

[9] I. Hofinger, M. Oechsner, H.-A. Bahr, and M. Swain, "Modified Four-Point Bending Specimen for Determining the Interface Fracture Energy for Thin, Brittle Layers," *International Journal of Fracture*, vol. 92, no. 3, pp. 213–220, 1998.